

Convection Indicator for Pre-Tactical Air Traffic Flow Management using Neural Networks

Aniel Jardines^{a,c,*}, Manuel Soler^{a,c}, Alejandro Cervantes^{b,c}, Javier García-Heras^{a,c}, Juan Simarro^d

^a*Department of Bioengineering and Aerospace Engineering*

^b*Department of Computer Science and Engineering*

^c*Universidad Carlos III de Madrid, Avda. Universidad 30, 28911 Leganes, Spain.*

^d*Agencia Estatal de Meteorología (AEMET), Valencia, Spain*

Abstract

Convective weather is a large source of disruption for air traffic management operations. Being able to predict thunderstorms the day before operations can help traffic managers plan around weather and improve air traffic flow management operations. In this paper, machine learning is applied on data from satellite storm observations and ensemble numerical weather prediction products to detect convective weather 36 hours in advance. The learning task is formulated as a binary classification problem and a neural network is trained to predict the occurrence of storms. The neural network results are used to develop a probabilistic based convection indicator capable of outperforming existing convection indicators found in the literature. Lastly, applications of the neural network based indicator in an air traffic management setting are presented.

Keywords: Thunderstorms, Air Traffic Management, Numerical Weather Prediction, Satellite Images, Machine Learning

*Corresponding author

Email addresses: ajardine@ing.uc3m.es (Aniel Jardines), masolera@ing.uc3m.es (Manuel Soler), acervant@inf.uc3m.es (Alejandro Cervantes), gcarrete@ing.uc3m.es (Javier García-Heras), jsimarro@aemet.es (Juan Simarro)

1. Introduction

Convective weather is a well known aviation hazard; turbulence, wind shear, lighting, and hail are elements arising in thunderstorms that can be catastrophic for aircraft. In Europe, convective weather, i.e. thunderstorms typically occur in the summer and coincide with a period of high air traffic demand on the airspace system. This combination of bad weather and high demand causes significant disruption to air traffic management operations resulting in delays throughout the network. In 2018, 25 % of the total delay in the European airspace was attributed to adverse weather, resulting in a total of 4.8 million minutes, the majority can be attributed to convective weather (EUROCONTROL, 2019). Using the estimated rate of 100€ per minute of delay (Cook & Tanner, 2015), the costs associated with the weather delay in 2018 can be quantified at 0.48 billion euros.

A key reason why thunderstorm phenomena are so disruptive is the difficulty of forecasting their birth and evolution. While some meteorological conditions are required for thunderstorm formation and can be forecast in advance, the specific location and timing of convective initiation triggers is harder to identify. As a consequence, thunderstorm prediction is usually performed using nowcasting. Nowcasting are short term predictions, typically 1 - 3 hours, based on extrapolation of sensor data such as Doppler radars or satellite (Wilson et al., 1998). However, extrapolation degrades rapidly as the forecasting horizon increases. One nowcasting system of particular interest for aviation is the Corridor Integrated Weather System (CIWS) (Evans & Ducot, 2006), which is in use in the US.

Due to the poor prediction precision of convective weather at time horizons greater than 3 hours, air navigation service providers and airlines typically do not make strategic modifications to their operational plans, instead preferring to make tactical adjustments in real-time according to the evolving weather situation. This reactive approach in handling convective weather events, is not conducive to coordination among multiple Air Navigation Service Providers (ANSP) and leads to inefficiency in the system.

The process of Air Traffic Flow Management (ATFM) aims at minimising network disruptions in the system by matching the airspace and airport capacity with the varying levels of traffic demand to ensure safety and efficiency throughout the airspace system. ATFM is a coordinated effort between multiple stakeholders including the Network Manager, national ANSPs, and aircraft operators. ATFM is a multi-phase iterative process beginning months

38 before the day of operations.

39 The pre-tactical phase of ATFM focuses on measures to be applied at least
40 one day prior to the day of operations. In this stage, analysis is performed
41 to refine capacity and demand estimates, and assess ATFM measures. The
42 outcome of this phase is a plan for the day of operations, known as the ATFM
43 Daily Plan (ADP) in Europe.

44 While weather condition are considered during this phase of ATFM, the
45 weather information available for input to the ATFM Daily Plan is limited.
46 In Europe, EUROCONTROL's Network Operations Portal provides a Daily
47 Network Weather Assessment, a document containing a brief written descrip-
48 tion of the general weather outlook for the Network, and severe weather alerts
49 for en route airspaces and airports. The weather assessment also contains
50 a series of static maps providing forecasts of temperature, winds and pre-
51 cipitation for the day. While this daily product is useful in providing some
52 awareness of the meteorological conditions for the day, it fails to capture
53 evolving weather phenomena such as convection. In order to effectively min-
54 imise the disruptions on the network, traffic managers require high confident
55 convective weather forecast with sufficient lead time.

56 In order to extend the lead time in thunderstorm prediction it is necessary
57 shift away from nowcasting methods and exploit the advances in Numerical
58 Weather Prediction (NWP) tools. NWP use computer simulations to model
59 the atmospheric processes at a computational grid. The fluid motion and
60 thermodynamic characteristics of the atmosphere are modeled using partial
61 differential equations, capturing interactions among neighboring grid cells
62 and calculating a broad set of atmospheric parameters for each grid cell.
63 These NWP products are able to predict the state of the atmosphere multiple
64 days into the future with fairly good accuracy. Indeed, the majority of the
65 weather forecast we use in our daily lives rely on NWP. However, NWP
66 have not traditionally been used for thunderstorm prediction because the size
67 and lifespans of thunderstorms are small compared with the spatiotemporal
68 resolution of medium-range NWP models.

69 Advances in weather science and high performance computing have greatly
70 improved the prediction skill of NWP in recent years. In our research we
71 set out to leverage these improvements and machine learning techniques to
72 predict thunderstorms using NWP at timescales (greater than 24 hours)
73 required for the pre-tactical phase air traffic flow management.

74 At shorter time horizons, machine learning and NWP have been used
75 successfully to improve nowcasting of thunderstorms. In (Mecikalski et al.,

76 2015), machine learning techniques were applied on satellite data to improved
77 their nowcasting algorithm’s ability to predict which cloud objects would
78 display convective initiation within the hour. Also, in (Li et al., 2019)
79 machine learning techniques are applied to Doppler radar images to predict
80 gale force winds. Also, in (Khandan et al., 2018) a Random Forest is used
81 to predict convection initiation for the next 6 hours from satellite and NWP
82 data. However, predictions at these time scales are not compatible with
83 pre-tactical ATFM operations.

84 Machine learning has also been applied on NWP data to predict thun-
85 derstorms for longer time horizons. In (Šaur, 2017), NWP and historical
86 weather data are used to train a back-propagation algorithm to predict con-
87 vective precipitation that may cause to flash floods over the Zlin region of
88 Czech Republic up to 24 hours in advance. In (Collins & Tissot, 2015), a
89 deep-learning neural network model is developed using cloud to ground light-
90 ning data to predict the occurrence of thunderstorms in certain regions of
91 Texas, US within 2 hour time steps at time horizons up to 15 hours. Random
92 Forest has also been applied on NWP to predict the probability of lightning
93 strike over the Alaskan tundra (He & Loboda, 2020). In (Simon et al.,
94 2018), thunderstorm occurrence within a 6 hour period is predicted over the
95 European eastern Alps up to 5 days in advance using generalized additive
96 models (GAMs) and gradient boosting with cloud-to-ground lightning data.
97 Convolutional Neural Networks have also been applied on NWP products to
98 predict multiple types of convective weather within a 6 hour period up to
99 72 hours in advance (Zhou et al., 2019). While these works have been suc-
100 cessful in using machine learning to predict convective weather, their specific
101 applications did not require spatial-temporal resolution nor the continental
102 scale geographic domain necessary for pre-tactical ATFM application. While
103 works predicting convective events with high spatial-temporal resolution do
104 exist (Spiridonov et al., 2020; Baldauf et al., 2011), they rely on physics-
105 based computational fluid dynamic models rather than machine learning,
106 and are limited in their geographical domain.

107 In this paper we apply machine learning to predict thunderstorm occur-
108 rence over a large portion of western Europe in hourly time steps at time
109 horizons up to 36 hours. An ensemble NWP with 0.25 degree spatial res-
110 olution and satellite observations from the EUMETSAT NWC-SAF Rapid-
111 Development Thunderstorm product are used to train a neural network to
112 provide the likelihood of convective weather. To the authors’ knowledge,
113 the use of satellite storm data is novel approach, previous works using ma-

chine learning to predict convective weather has relied on cloud-to-ground lightning.

Model results are used to create a convection indicator that enables the consideration of thunderstorms during the pre-tactical phase of ATFM. The novel indicator is compared with an existing convection indicator found in the literature. The remainder of this paper is organized as follows. Section 2 presents an overview of the data used, while details of the neural network are provided in Section 3. Next, results are presented in Section 4, followed by examples of model application within an ATFM context in Section 5. Finally, a summary is provided in Section 6 where conclusions and future work are discussed.

2. Weather Data

Convection is a vertical phenomena in the atmosphere created by the uneven heating of the Earth's surface due to solar radiation. Heat from the Earth's surface warms the air directly above it, causing the air to expand, becoming less dense than the surrounding air, and creating thermal columns of rising air. If moisture is also present, the warm moist air will rise and in the processes cool and condense. If sufficient instability is present in the atmosphere, this process can form extensive towering cumulonimbus clouds creating ideal conditions for thunderstorms. Convective storms can become quite extensive and be observed from space.

In developing the convection prediction model, data from ensemble NWP forecasts and satellite thunderstorms observations are used. Given the lead times required for pre-tactical ATFM, the model input is provided by ensemble NWP forecasts, as these are available 36 hours in advance. Satellite image data is used for training and evaluation of the model as it provides an accurate representation of convective events. The data used is from June 2018 with a geographical domain covering vast portions of western Europe and northern Africa as seen in Figure 1.

2.1. Ensemble NWP

Ensemble probabilistic forecasting is a technique used to provide an estimate of the uncertainty associated with predictions of the atmosphere. Rather than forecasting one future scenario as in traditional NWP, multiple future scenarios are created, using a variety of techniques including perturbing initial conditions, running multiple models, or using different combina-



Figure 1: Geographical domain of forecast and observational weather data.

149 tions of physical parameterization schemes. The perturbation techniques are
150 inline with the observational errors in the current state of the atmosphere. An
151 assumption in using ensemble forecasts is that the probability of occurrence
152 for each member is equally likely. A priori, there is no way of knowing which
153 members will more closely resemble actual conditions. Furthermore, one en-
154 semble member may be closest to the truth at a given geographical location,
155 but this need not be the case at another location (Palmer et al., 2006).
156 The spread of the members will reflect the predictability of the atmosphere,
157 with a larger deviation between members indicative of a less predictable at-
158 mosphere. The goal of the ensemble system is to capture reality within the
159 range of predictions. The ensemble NWP data used in this research comes
160 from European Centre for Medium-Range Weather Forecasts (ECMWF) En-
161 semble Prediction System (EPS). The EPS product is comprised of a control
162 member, using the most accurate estimate of the initial conditions, plus 50
163 perturbed members. The forecasts are released twice a day at 00:00 and 12:00
164 UTC and provide a prediction of the weather up to 15 days ahead (Molteni
165 et al., 1996).

166 In developing our model we use data from the 50 perturbed members,
167 focusing on the forecast provisions for the next 36 hours in 1 hour steps. The
168 spatial resolution of the EPS perturbed members is a quarter of a degree
169 in latitude and longitude, this equates to roughly 15 nautical miles between
170 grid points.

171 In selecting the NWP parameters for training or model we chose those
172 that could best capture the physics of convective weather and thunderstorms.
173 Our selection was guided based on the principle that thunderstorms are most
174 likely to occur under the following conditions (Oxf, 2015):

- 175 • Lifting force or trigger mechanism to produce early saturation of air. In
176 convective storms, this trigger action is typically caused by heat from
177 the earth’s surface causing moist air to rise.
- 178 • Sufficient moisture in the atmosphere to form and maintain the cloud.
- 179 • Atmospheric instability determined by the vertical temperature profile
180 or lapse rate.

181 With these conditions in mind, 18 NWP parameters from the EPS were
182 selected to train the NN model. Besides these 18 NWP parameters, we also
183 included additional parameters to train our model. The parameter *hour of*
184 *the day* was added to account for the weather patterns that occur throughout
185 the diurnal cycle. The time horizon or *range of forecast* was also added, this
186 parameter describes how far into the future a prediction is made. We hy-
187 pothesized that our model may give more weight to certain parameters based
188 on the range. Additionally, we also trained the model with the Convective
189 available potential energy (cape) parameter values from the three previous
190 time steps of the ensemble product because large values of cape correlate
191 with time periods leading up to the storm, rather than during the storm
192 itself. This provided us with a total of 23 input parameters (18 ECMWF
193 parameters + 1 Hour of day + 1 Range of forecast + 3 time lagged CAPE
194) to train our model. The complete list of parameters and abbreviation is
195 provided in Table 1.

196 2.2. Satellite Data

197 Geostationary satellites with orbital periods that match the Earth’s rota-
198 tion allow for continuous observation of specific regions. Visual and infrared
199 satellite imagery captures vital information regarding cloud cover, water va-
200 por and temperature that allow for monitoring and tracking of weather.

201 The Rapid-Development Thunderstorm (RDT) product was developed
202 by Météo-France within the EUMETSAT NWC-SAF framework. The RDT
203 algorithm employs primarily geostationary satellite data to provide informa-
204 tion about clouds related to significant convective systems from the mesoscale

Table 1: Total list of parameters used to train model.

Parameter	Short Name
2 metre dewpoint	2d
2 metre temperature	2t
convective available potential energy	cape
convective available potential energy 1 hour before	cape-1
convective available potential energy 2 hours before	cape-2
convective available potential energy 3 hours before	cape-3
convective inhibition	cin
convective precipitation	cp
convective rain rate	crr
height of convective cloud top	hcct
hour of day	hour
K index	kx
large scale precipitation	lsp
large scale rain rate	lsrr
surface latent heat flux	slhf
surface pressure	sp
surface sensible heat flux	sshf
range of forecast	range
total cloud cover	tcc
total column water	tcw
total column water vapor	tcwv
total totals index	totalx
geopotential	z

205 (200–2000 km) down to tenths of kilometers (Lee et al., 2020). The RDT
 206 product outputs storm information on a 15 minute interval. For each cloud
 207 cell, the RDT product defines a series of parameters capturing the loca-
 208 tion, shape, cloud top, movement, severity, and life cycle phase. Despite the
 209 rich characterization of thunderstorms by the RDT product, only the loca-
 210 tion and shape information of convective cells is used to create the labeled
 211 ”truth” training data required for supervised learning type problems.

212 *2.3. Data Integration*

213 Train, validation and test data sets are created by integrating the NWP
214 forecast and the RDT satellite images. By projecting the NWP grid onto
215 the higher resolution satellite images and identifying the grid points within
216 the RDT storm polygons it is possible to express the data using a common
217 spatial resolution of .25 degree x .25 degree. To reconcile the differences in
218 the temporal resolution, 1 hour for the NWP predictions versus 15 minutes
219 for the RDT observations, a grid point is classified as convective if a storm
220 observation is present during any of the four observations instances within
221 the hour. In this way a binary training target function is constructed repre-
222 sentative of storm cell occurrence at a grid location within the hour. Figure
223 2 shows an example of how four satellite images are processed to establish
224 from the target function.

225 Because we are interested in a time horizon of 36 hours, and forecasts are
226 released every 12 hours, different range forecasts valid for the same time are
227 used to train, validate and test the model. Having data at varying forecast
228 ranges will allow us to analyse how the forecast degrades with increasing time
229 horizon.

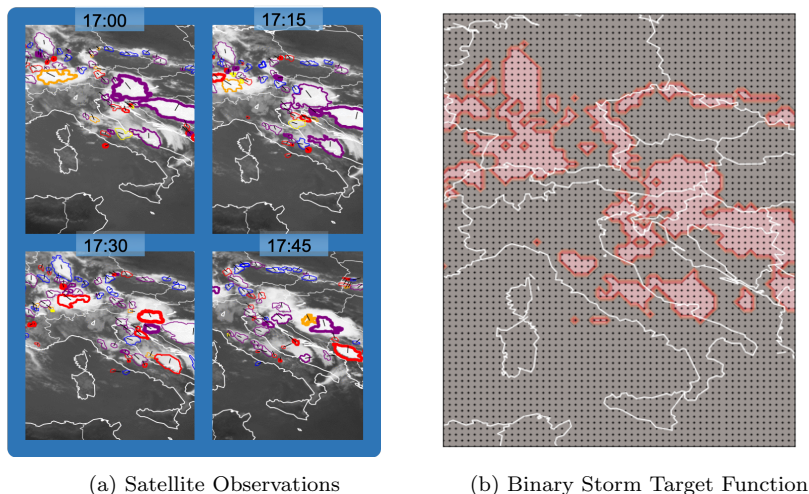


Figure 2: RDT satellite observations and resulting target function for thunderstorms occurring at 17:00 on June 8th, 2018.

230 3. Methodology

231 Before undertaking this study, a series of smaller preliminary case studies
232 was conducted on a limited data set. Multiple machine learning models were
233 developed using storm observations from the RDT product and one ensemble
234 member from the ECMWF EPS product. The NWP product consisted of
235 a 0.25 degree spatial grid, a 3 hour time step and 48 hour forecast range.
236 Eight days of worth of data, June 4th - June 11th, were split to create
237 train, validation and test data sets. Results from the study showed that
238 a Neural Network architecture was superior than other methods including
239 Logistic Regression, Decision Tree, and Random Forrest. It was assumed
240 that the advantage in prediction skill for the NN method would hold true
241 on a data set incorporating all 50 members and smaller time step of 1 hour.
242 A Convolutional Neural Networks (CNN) architecture was also considered,
243 however given the high resolution of our data set; hourly time steps, 36 hour
244 forecast range, .25 degree spatial resolution, a geographical domain of western
245 Europe, and the 50 ensemble members, using a CNN approach supposed a
246 significant increase in computational cost. While a CNN methodology may
247 be able to capture correlation among neighboring grid points, it is assumed
248 that the physical process behind these interactions is already captured to
249 some degree within the NWP model. As a result, for the purposes of training
250 the neural network model, the data from each grid point is assumed to be
251 an independent data sample. Also, during training each forecast member is
252 treated individually. In this way, during training the model sees 50 separate
253 data samples from each grid point in the ensemble forecast. The intention is
254 for the model to benefit from ensemble distribution of parameters and adjust
255 the neural network node weights accordingly.

256 The convection predictive model is trained to predict the probability of a
257 thunderstorm occurring at given location and time. Only the 23 parameters
258 defined in Table 1 are considered in making a prediction. In evaluating the
259 model, each forecast member is evaluated separately, and results are averaged
260 over the 50 members to obtain a probability.

261 For this study an integrated data set of EPS forecast and RDT observa-
262 tions covering the month of June 2018 is used. From the 30 days in June, 16
263 days are selected for training, 7 days for validation and 7 for testing, exact
264 dates used for each data subset can be seen in Table 2. This partition was
265 preferred over a sequential split to ensure sufficient convective samples in
266 each subset. It is acknowledged that having a test data set embedded within

267 the training data could introduce look-ahead bias in our results, however
 268 considering the NWP forecast is provided in hourly time steps and that the
 269 lifespan of convective events is on the order of hours, each day is treated
 270 independently. We assume that the convective events occurring on a specific
 271 day are independent from those occurring on a separate day. While tem-
 272 poral correlations exist in the atmosphere over consecutive days, we assume
 273 these correlations are more likely to be inherent within the NWP input than
 274 learned by the model.

275 3.1. Neural Network Model

276 The learning task of predicting convective weather was formulated as
 277 a binary classification problem. Based on the 23 inputs derived from the
 278 NWP forecast our model was trained to classify a grid-point as either con-
 279 vective (class 1) or not-convective(class 0). It is important to note that the
 280 model does not consider the latitude-longitude of the grid-point, providing
 281 a location-independent prediction based only on the physical NWP param-
 282 eters.

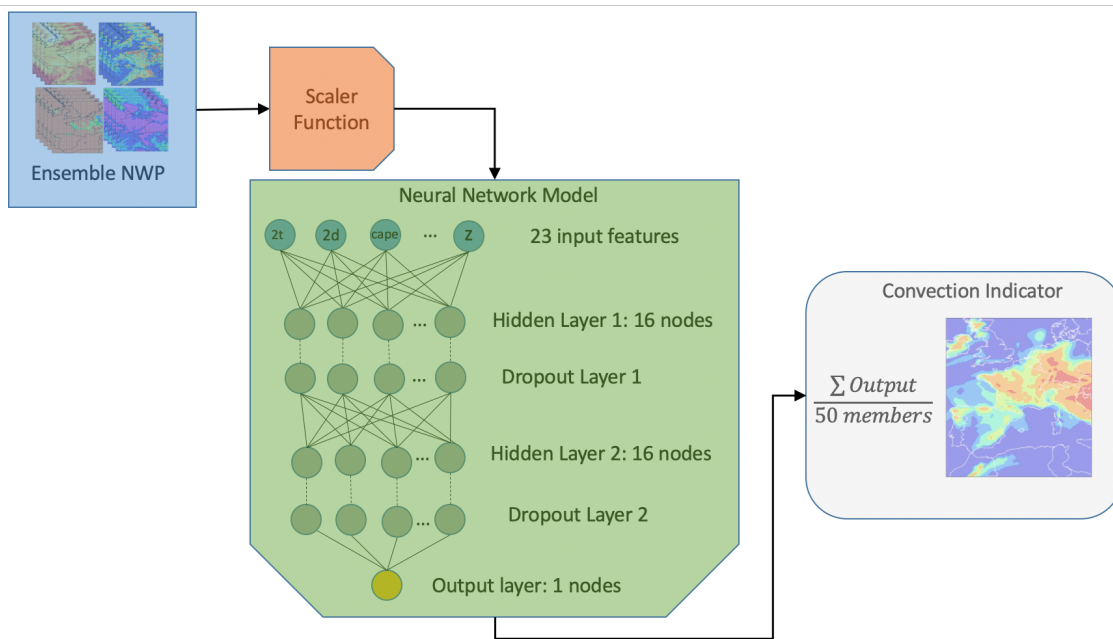


Figure 3: Schematic of neural network model, showing data flow from ensemble NWP to convection indicator.

283 A Multi-layer Perceptron (MLP) neural network was created using the
 284 python keras library to fit the data. The 23 NWP features were normalized
 285 using a standard scaler function before fitting the model to account for the
 286 order of magnitude differences between the values. The model consisted of
 287 the input layer with 23 nodes, two hidden layers of 16 nodes each and the
 288 output layer containing one node. The nodes in the hidden layers of the
 289 model used a Rectified Linear Unit activation function, while the node in the
 290 output layer used a Sigmoid activation function. By having a Sigmoid output,
 291 the model predicts a value between 0 and 1 instead of binary. This output
 292 value is representative of the confidence the sample is convective (class 1).
 293 Additionally, during training dropout layers of fraction 0.2 were introduced
 294 after each hidden layer. Dropout is a technique to prevent over-fitting of the
 295 model by randomly ignoring a fraction of the nodes during each iteration
 296 of training, in effect reducing the interdependent learning between neurons
 297 (Srivastava et al., 2014). In figure 3 a schematic representation shows the
 298 model architecture and data process from EPS data to convection indicator.

299 It is important to note that the data was highly imbalanced, with roughly
 300 90 % of the samples belonging to the non-convective class. To account for
 301 this imbalance, class weighting factors were applied during training. By im-
 302 plementing a class weighting factor, the binary cross-entropy loss function
 303 used for training assigned higher values to instances of the minority convec-
 304 tive class. This reduces the impact of the majority class in the loss func-
 305 tion, preventing the generation of models that basically predict the majority
 306 (non-convective) class for all samples. The weighted binary cross entropy
 307 loss function is defined in Equation 1, where w_i is the weight factor for each
 308 class, t is the truth value of 0 or 1, and p is the probability of the sample
 309 belonging to the convective class.

$$CE = -w_i \sum_{i=0}^{C'-1} t_i \log(p_i) = -w_i [t \log(p) + (1 - t) \log(1 - p)] \quad (1)$$

310 4. Results

311 In this section we present the results of the neural network model for the
 312 seven days in in our test data set. For comparison we also present the results
 313 from an existing NWP based convection indicator, in our discussion we will
 314 refer to this indicator as the baseline. A brief description of the baseline
 315 indicator is provided below.

Table 2: Dates used for training, validation and testing

Training		Validation	Test
Jun-01	Jun-02	Jun-03	Jun-04
Jun-05	Jun-06	Jun-07	Jun-08
Jun-09	Jun-10	Jun-11	Jun-12
Jun-13	Jun-14	Jun-15	Jun-16
Jun-17	Jun-18	Jun-19	Jun-20
Jun-21	Jun-22	Jun-23	Jun-24
Jun-25	Jun-26	Jun-27	Jun-28
Jun-29	Jun-30		

316 *4.1. Baseline Indicator Description*

317 An existing convection indicator used within an aviation context was
 318 found in the literature (González-Arribas et al., 2019). The indicator re-
 319 lies on two parameters from a numerical weather prediction product; Total
 320 Totals Index and Convective Precipitation . Total Totals Index (*totalx*) is
 321 the temperature and moisture gradient in the lower levels atmosphere and
 322 an indication of instability. Convective Precipitation (*cp*) is the accumulated
 323 water that falls to the Earth’s surface that is generated by convection. Con-
 324 vection can be defined as an area where there is atmospheric instability and
 325 precipitation. Thus we can evaluate each point of the numerical weather
 326 prediction model for convection using the logistic expression in Equation 2.

$$Convection = (totalx > TT_{TH}) \wedge (cp > 0) \tag{2}$$

327 where TT_{TH} is defined as the Total Totals Index threshold value. This
 328 threshold value can be associated with various levels of convection. The cor-
 329 relation between threshold value and convection severity is provided below.

- 330 • 44-45 isolated moderate thunderstorms
- 331 • 46-47 scattered moderate / few heavy thunderstorms
- 332 • 48-49 scattered moderate / few heavy / isolated severe thunderstorms
- 333 • 50-51 scattered heavy / few severe thunderstorms and isolated torna-
 334 does

- 335 • 52-55 scattered to numerous heavy / few to scattered severe thunder-
336 storm / few tornadoes
- 337 • 55+ numerous heavy / scattered severe thunderstorms and scattered
338 tornadoes

339 Equation 2 is used to evaluate each grid point of the NWP. If both condi-
340 tions in the logistic expression are met the grid point location is classified as
341 convective (1), if the conditions are not met the location is classified as non-
342 convective (0). These binary values are then averaged over the 50 ensemble
343 members to provide the final Baseline Indicator score.

344 In our application of the baseline indicator we will assume a Totals Total
345 Index threshold value of 44, and rather than using cp , which gives an accu-
346 mulated value of convective precipitation since the forecast release, we will
347 utilize the convective rain rate (crr). It is important to note that while cp
348 is an accumulated parameter, crr is considered an instantaneous parameter,
349 and not representative of the rain rate over the entire time step. Nonethe-
350 less, using the parameter crr instead of cp will better account for convective
351 weather at discrete time steps in the forecast. The expression used to calcu-
352 late the baseline convection indicator is provided in Equation 3.

$$Convection = (totalx > 44) \wedge (crr > 0) \quad (3)$$

353 4.2. Model Comparison

354 The effectiveness of our NN convection indicator is compared with the
355 baseline indicator using a receiver operating characteristic (ROC) curve. A
356 ROC curve is a technique used to evaluate binary classifiers by plotting the
357 sensitivity, or true positive rate (TPR), against (1-specificity), or the false
358 positive rate (FPR), for various threshold settings (Mandrekar, 2010). The
359 TPR provides the probability of detection, and the FPR provides the prob-
360 ability of false alarm. The ideal classifier would have a curve close to the
361 upper left corner of the graph and maximizing the area under the curve
362 (AUC). The diagonal line dividing the ROC space represents a random clas-
363 sifier, points above the line indicate the classifier performs better than ran-
364 dom guessing. Model performance can be tuned by selecting a threshold
365 value on the curve, which leads to a specific pair (FPR,TPR). In practice,
366 the selection of a threshold value is linked with the amount of risk a user is
367 willing to assume. A low threshold would increase the likelihood of capturing

368 the thunderstorms, while also overestimating their presence in the airspace
 369 (false alarm). However, choosing a high threshold value would minimize the
 370 false alarm rate, at the risk of missing a portion of the storms. In presenting
 371 the results, rather than defining a threshold value, the raw indicator values
 372 are compared. A probabilistic representation of the indicator is preferred for
 373 an ATFM application allowing the user to evaluate the risks in making a
 374 decision.

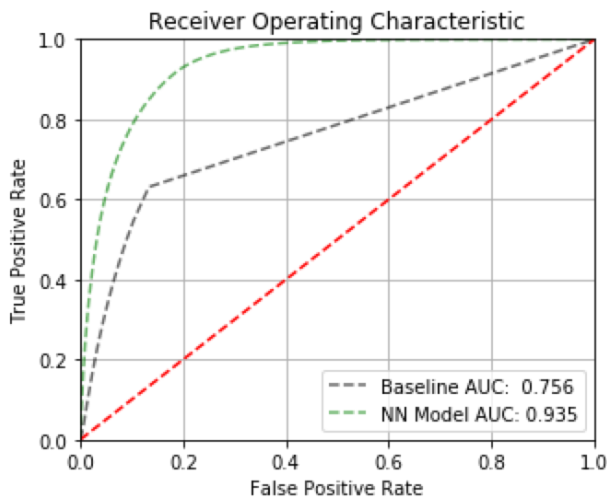


Figure 4: ROC curve comparing performance of baseline and neural network indicators for entire test data set.

375 In Figure 4 results are compared between the NN and baseline indicators
 376 for the 7 days in the test data set. From the figure it is evident that the NN
 377 model outperforms the baseline indicator given the greater value of AUC.
 378 Moreover, because the NN curve is always above the baseline curve, the NN
 379 model outperforms the baseline independently of a chosen threshold value.
 380 It is important to note that the AUC value is dependent on the particular
 381 data set being analyzed. The NN model is good at identifying areas without
 382 convection (true negatives), thus analysis of days with few convective storms
 383 will yield greater AUC values.

384 In Figure 5 results are presented for the entire test data set using the
 385 prediction score by class. Histograms are provided for the baseline and neural
 386 network model. In the graphs the convection class is shown in red, while the
 387 non-convective class is shown in grey. Given the class imbalance in the test

388 data set, the distributions have been normalized so that the two classes oc-
 389 cupy the same area in the graphs. Ideally, we would like the two distribution
 390 completely separated, with the non-convective (grey) distribution closer to a
 391 prediction score 0 and the convective distribution (red) closer to a prediction
 392 score of 1. The histogram on the left, shows the baseline model does a good
 393 job at evaluating the non-convective areas with a low probability score. How-
 394 ever it is also unable to distinguish a large portion of the convective areas
 395 from non-convective areas. The histogram on the right, corresponding to the
 396 NN model shows less overlap between the two class distributions indicating
 397 better performance.

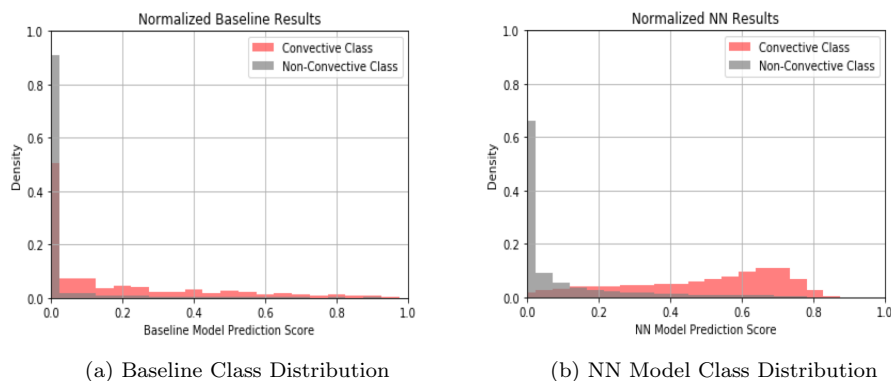


Figure 5: Normalized histograms showing the class distributions by predictive score of baseline and neural network models for test data set.

398 Figure 6 shows a map representation of the target function alongside the
 399 baseline and neural network model predictions for a geographical domain
 400 centered over Italy. ROC AUC values corresponding to the data portrayed
 401 on the maps are provided. From the figure we can see that while the baseline
 402 correctly identifies some areas where storms will develop, it tends to provide
 403 low prediction scores and there is a large portion of the convective areas
 404 that it misses completely. The NN model although may tend to slightly
 405 overestimate the storms, the prediction probability seems to be more gradual
 406 for the convective areas. A traffic manager wanting reroute traffic flows
 407 around convective weather based on the predictive score from the indicators,
 408 would get a more accurate representation of the convective regions in the
 409 airspace by using the neural network based convective indicator.

410 In Figure 7 results for the NN convection indicator are shown for the
 411 entire geographical domain. The figure shows the target function and model

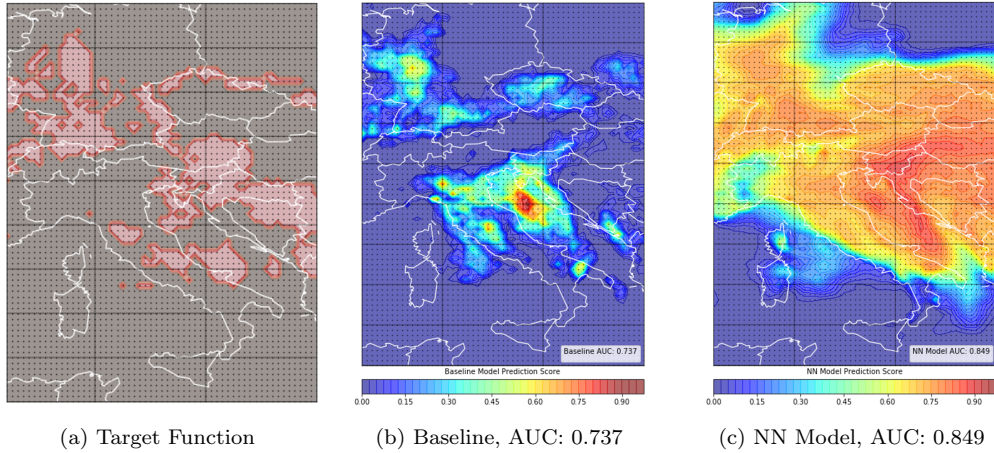


Figure 6: Binary thunderstorm target function compared with baseline and neural network model predictions for 17:00 UTC on June 8th, 2018 (Forecast range: 17 hours).

412 predictions for June 20, 2018 from 13:00 - 16:00 UTC based on the forecast
 413 from June 19, 12:00.

414 The map representation of results from Figures 6 and 7 show the convective
 415 predictions made on the day before operations. Continuous monitoring
 416 of an upcoming convective situations is necessary for an ATFM operations,
 417 therefore it is important to understand how the predictions of the indicator
 418 change over the prediction time horizon. In Figure 8, we show how the
 419 ROC curves for both indicators behave given different forecast ranges. From
 420 the figure can see that the AUC for the NN model remains fairly constant
 421 at ranges up to 24 hours, and degrades slightly when extended to 36 hours.
 422 These results indicate that the quality of the results do not degrade at the
 423 time scales required for the pre-tactical phase of ATFM.

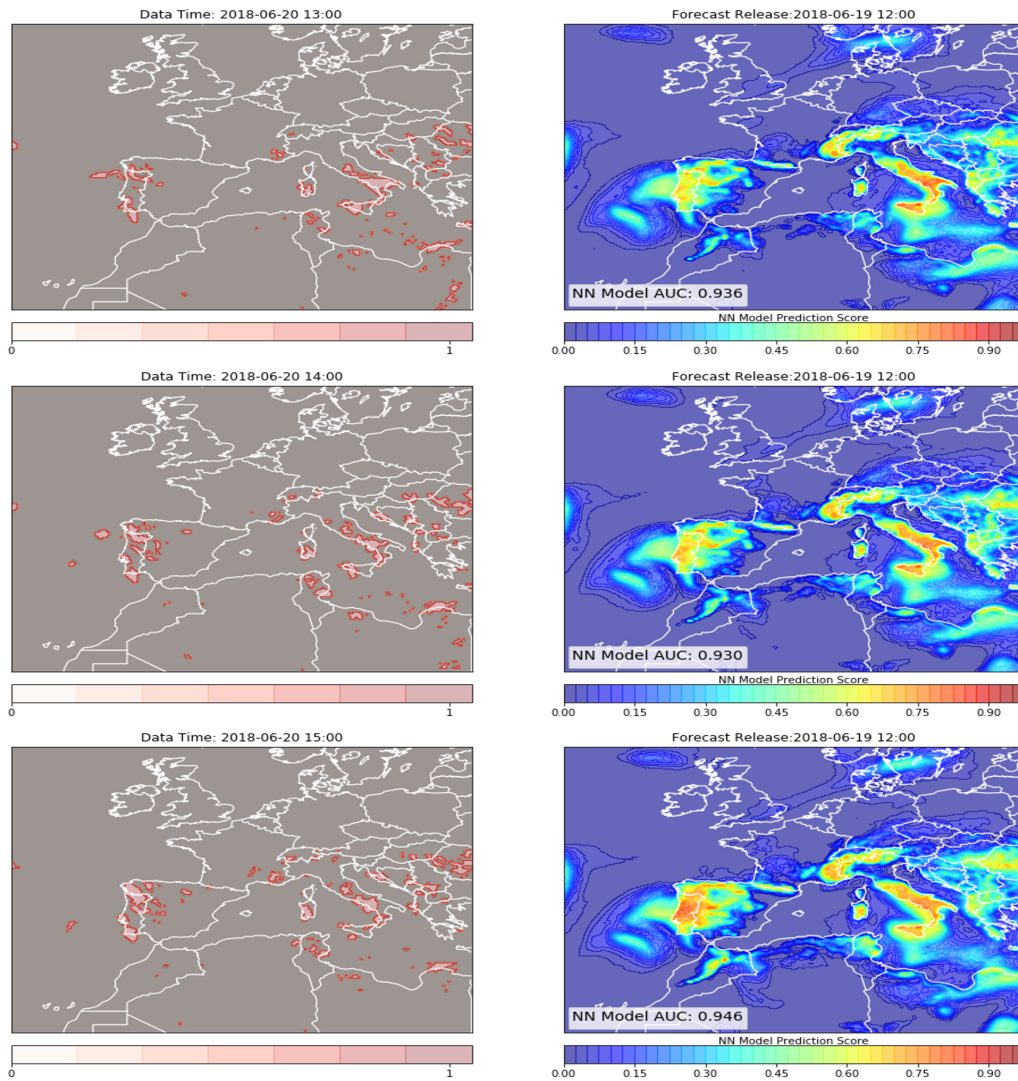


Figure 7: Convection prediction for June 20, 2018 made on June 19, 12:00.

424 *4.3. Study of Feature Relevance*

425 A permutation analysis was performed to understand which of the ECMWF
 426 EPS parameters were most important in predicting convection. The theory
 427 behind the permutation analysis is to measure the importance of a feature by
 428 calculating the degradation of model performance after permuting the fea-
 429 ture. A more important feature will increase the model error after shuffling
 430 its values because the model relies on this feature to make its prediction,

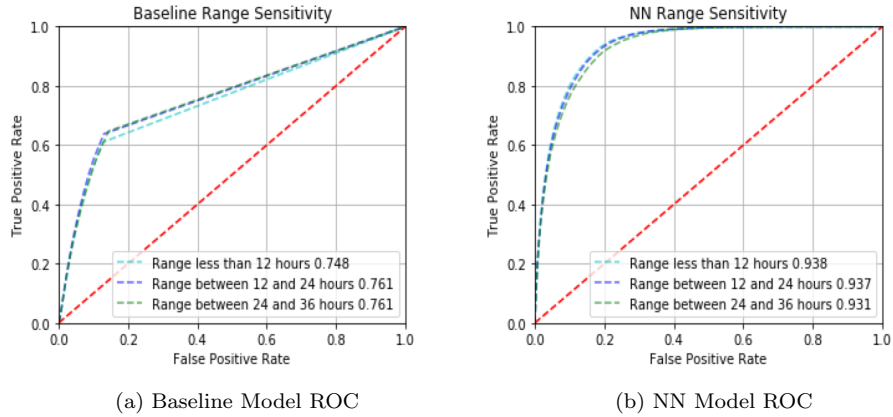


Figure 8: ROC curves showing model sensitivity to forecast range variation.

431 while shuffling the values of a less important feature will have little impact
 432 on the model error. This technique was first introduced specifically for ran-
 433 dom forest models (Breiman, 2001), and later expanded to a model-agnostic
 434 version (Fisher et al., 2019).

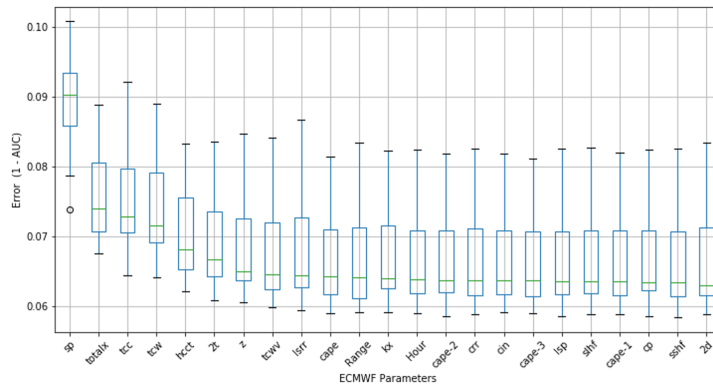


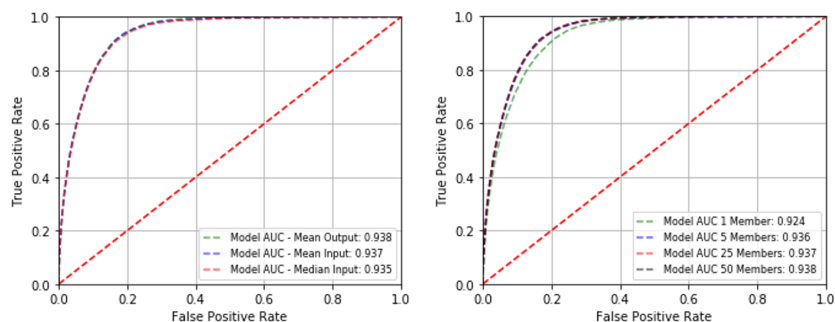
Figure 9: Error in AUC after permutation of surface ECMWF parameters.

435 In our analysis we measure the model error by the increase in 1 - AUC.
 436 Figure 9 shows the results of a permutation analysis performed on several
 437 batches from the test data set. For each parameter we are able to see the
 438 distribution of error associated with permuting that feature. From the figure
 439 we see can see that permuting the surface pressure (sp), total totals index
 440 (totalx), total cloud cover (tcc) and total column water (tcw) parameters

441 produce the greatest error. Interestingly enough we can relate these paramete-
 442 rters to the already mentioned conditions that are favorable to thunderstorms;
 443 moisture (tcc,tcw), instability (totalx), and lifting force (sp). This type of
 444 analysis will be useful in selecting additional NWP to include in future ver-
 445 sions of out model.

446 4.4. Study of Model Sensitivity to Ensemble Data

447 In this section a series of case studies are presented to better understand
 448 the model sensitivity to the ensemble data. A random subset of the test
 449 data set is selected to evaluate the model for various cases. In the first case,
 450 various methods of aggregating the ensemble data are compared. Evaluating
 451 the model on each individual member and averaging the outputs is compared
 452 with taking the mean of each parameter prior to evaluating the model. Ad-
 453 ditionally, results are also shown for using an input based on the the median
 454 value for each parameter. In Figure 10a it is shown that while the various en-
 455 semble aggregation methods do not impact the results, averaging the output
 456 is slightly better.



(a) Comparison of ensemble aggregation methods for model evaluation. (b) NN model results using a subset of the ensemble members.

Figure 10: ROC curves showing model sensitivity to ensemble data.

457 In the second case, we explore how model results compare if a subset of
 458 the ensemble members are used to make a prediction. For this study the
 459 same random subset of the test data is evaluated multiple times using a
 460 limited number of ensemble members. Results are shown when the model is
 461 evaluated using only 1, 5, and 25 randomly selected members and compared
 462 with results when using the entire ensemble. From Figure 10b, it is evident
 463 that results improve as the number of ensemble members used is increased,

464 although the incremental improvement is diminished as more members are
465 added.

466 In the last case study, the model performance is compared on four data
467 sets; the training, validation and test data partitions, as well as an addi-
468 tional data set comprised of ECMWF predictions for the month of July 2018
469 using only 10 ensemble members. Within each of these four data groups,
470 50 randomly selected hourly predictions we used to evaluate the model. A
471 ROC curve comparing the model performance across the four data sets is
472 provided in Figure 11, from the figure we can see the model classification
473 skill is similar for all data sets. It is important to highlight the performance
474 for the July data set comprised of only 10 ensemble members is similar to
475 that of the other data sets which comprised of all 50 members, this further
476 confirms the results presented in Figure 10b. Finally, given that the ROC
477 curve AUC value is sensitive to the weather conditions within each data set,
478 Figure 12 shows map representations of the July data.

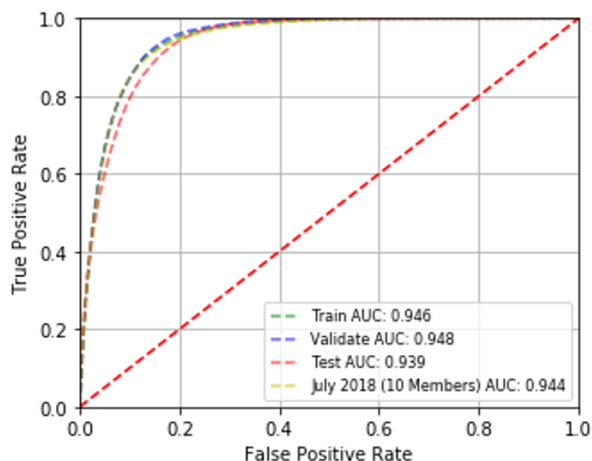
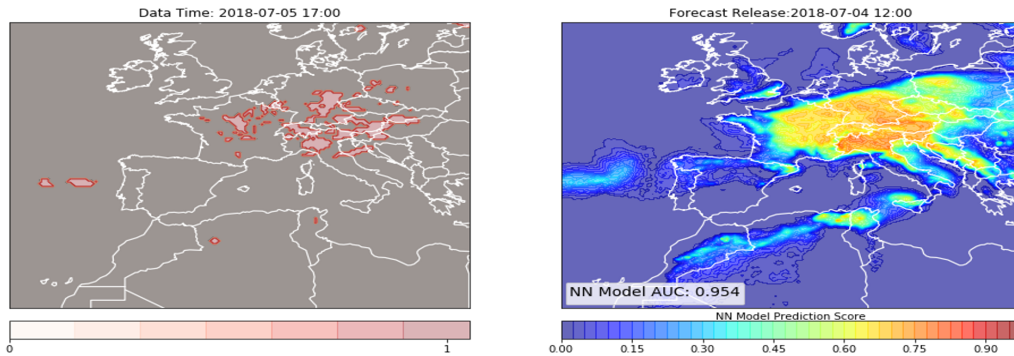


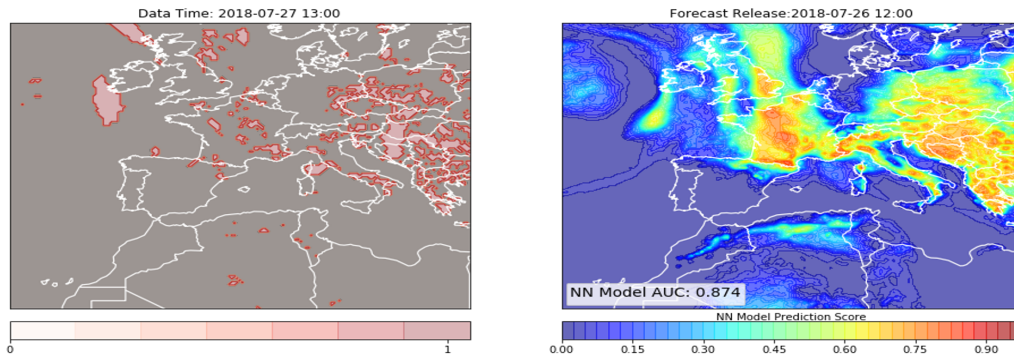
Figure 11: ROC curve comparing NN model evaluation using subsets of training, validation and test data sets. An additional data set based on forecast predictions for July 2018 is also compared.

479 5. ATFM Application

480 In this section we present an example of possible application of the neural
481 network indicator in an ATFM operational setting. The objective of this work
482 is to provide traffic managers with awareness of where and when convective



(a) Prediction for July 5, 17:00 (Range: 29 hours)



(b) Prediction for July 27, 13:00 (Range: 25 hours)

Figure 12: Convection predictions for July 2018 based on 10 members from ensemble.

483 weather will develop. Perhaps, the most obvious application would be to
 484 overlay the convective prediction on a map of structured airspace, in this way
 485 traffic managers could have information on which sectors will be impacted
 486 be convective weather. A conceptual map of our indicator overlaid atop
 487 the European Area Control Centres (ACC), ACCs establish the areas of
 488 jurisdiction for the various control units in the European airspace. In Figure
 489 13 we compare the actual storm situation as captured by the RDT data with
 490 the convection prediction of the NN indicator. From the figure we can see
 491 that there was storm activity in multiple Spanish ACCs on June 28th, 2018
 492 at 15:00 UTC, the neural network indicator prediction one day before the
 493 day of operations (D-1) at noon is able to capture the general area of the
 494 storms. In another application the information is presented in a manner that
 495 is specific for a unit of airspace. In this example we focus on the Marseille
 496 ACC, a region of airspace responsible for 15.2% of ATFM delay in Europe in

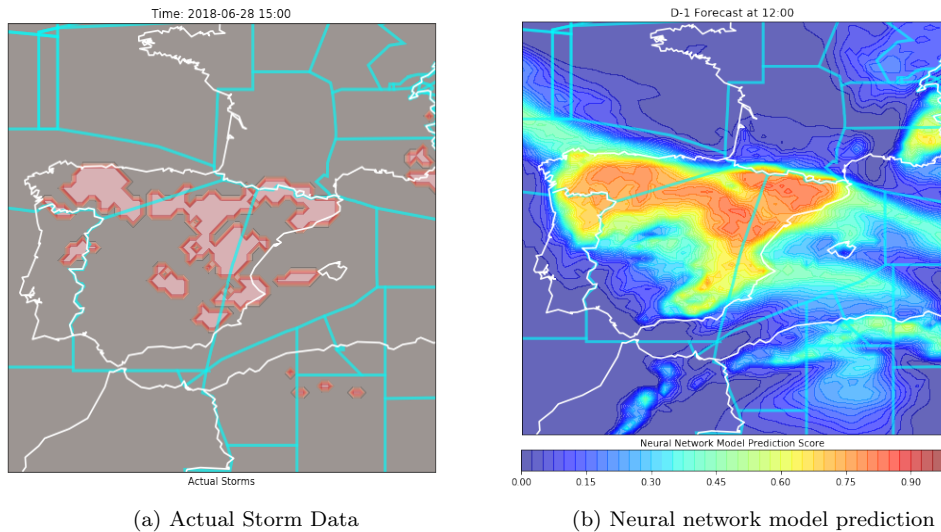
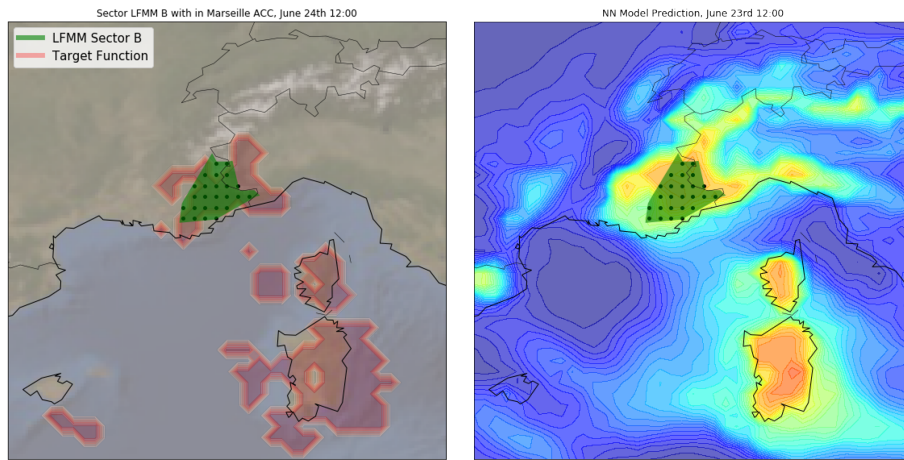


Figure 13: Convection prediction captures storms in Spanish ACCs one day before.

497 2018 (EUROCONTROL, 2019). Specifically we focus on Sector B within the
 498 Marseille ACC as shown in Figure 14. Based on the NWP resolution, the area
 499 covering this unit of airspace can be represented with 25 grid points. Using
 500 the model predictions from these 25 points it is possible to define a metric
 501 to evaluate the convection situation in the sector. In Figure 15 multiple
 502 convection metrics based on the baseline and NN model are compared with
 503 the RDT data from June 24th 2018. Figures 15a and 15b show metrics based
 504 on the average indicator value over the 25 points for the baseline and NN
 505 model. In Figures 15c and 15d the metric is based on the NN model output
 506 and the percentage of grid points exceeding specific thresholds. The various
 507 dashed colored lines corresponding to the left y-axis relate to the calculated
 508 convection metric with the Marseille ACC for various forecast releases on
 509 the day before operations (D-1) and the day of operations (D). The solid
 510 black line corresponding to the right y-axis, shows the percentage of airspace
 511 region with storms according to the target function.

512 From Figure 15 it is evident that while all metrics capture some convec-
 513 tive activity, using the neural network model results with an applied thresh-
 514 old better captures the convective situation within LFMM Sector B. It is
 515 imagined that the neural network model output can be used to define con-
 516 vection metrics within European airspace to continuously monitor and assess
 517 the weather situation. Further analysis is needed to better understand how



(a) Target function representation

(b) Neural network model prediction

Figure 14: Marseille Sector B and convective weather situation on June 24th, 2018 at 12:00 and prediction (Range: 24 hours.)

518 these convection metrics impact ATFM attributes such as airspace capaci-
 519 ties, traffic demand, and weather regulations. Understanding the relationship
 520 between weather prediction and the impact on the traffic would allow traffic
 521 managers to make better decisions during the pre-tactical phase of ATFM.

522 6. Summary and conclusions

523 In this paper we have applied machine learning techniques to predict
524 convective areas within the next 36 hours. By combining data from satellite
525 storm observations and ensemble NWP products, a neural network algorithm
526 is trained to predict the occurrence of convective weather. The NN model
527 is able to outperform an existing convection indicator currently used in avi-
528 ation applications. Analyses of the model on a test data set indicate that
529 model performance does not degrade significantly for forecast ranges up to
530 36 hours. Additional evaluation of the model showed that model perfor-
531 mance is maintained when evaluating on a subset of the ensemble forecast.
532 Furthermore, a permutation analysis was completed to detect which EPS pa-
533 rameters are most relevant to convection prediction. Findings confirm those
534 parameters related to the physical process of convection, correspond to the
535 most relevant features of our model. Lastly, examples are provided for the
536 use of the indicator in an ATFM operational setting. Visualization of model
537 predictions show that the model is able to accurately predict regions where
538 convection will develop. Model predictions are used to develop convection
539 metrics and used to evaluate the weather situating within a specific sector
540 within the Marsielle ACC and compared against storm observations. This
541 analyses suggest that applying a threshold atop of the model predictions can
542 improve the detection of convective weather.

543 Despite these initial positive results, several areas of improvement remain
544 to be tackled in future efforts. One area of improvement is to move away
545 from the assumptions of treating each ensemble member and each grid point
546 as independent. It is acknowledged that more efficient use of the NWP
547 ensemble product would be to provide model input that jointly considers
548 all ensemble members. Additional data processing and integration of the
549 NWP data is required to provide the model with an input representative
550 of all ensemble members. Furthermore, other model architectures including
551 Convolution Neural Networks and Long Short-Term Memory Networks need
552 to be considered to better extract the spatial-temporal relationships within
553 the data.

554 Another area of improvement is the quality of the data that is used to
555 train the models. Making use of higher resolution NWP products as well
556 as additional parameters at various atmospheric levels could provide im-
557 proved model inputs. Additionally, we could also incorporate other sources
558 of convection observation data, such as radar or lightning, to provide the

559 model with a more precise target function to be used during training. Fu-
560 ture research efforts should focus on how to best integrate these various data
561 sources.

562 Furthermore, the model uses a binary classification scheme to predict the
563 probability that convection will occur. However, in the future we hope to
564 expand the model to also identify key characteristics associated with con-
565 vection, such as storm severity and cloud top altitude; both relevant infor-
566 mation in an air traffic flow management context. These efforts could be
567 accomplished by moving away from a binary representation and elaborating
568 a more sophisticated target function able to capture those storm character-
569 istics that have a major impact on ATFM operations.

570 Lastly, an important step in the application of the model in an ATFM
571 operation setting is further refinement of raw model output in order to pro-
572 vide traffic managers with simple and relevant information. One possible
573 solution is to translate the model output into a color-scheme, similar to what
574 is currently in use today.

575 The goal of this research is to provide traffic managers with improved
576 convective weather information at time frames compatible with pre-tactical
577 ATFM planning. While this objective has been achieved to some extent,
578 further research efforts are still needed to relate the convection prediction
579 with ATFM metrics such as airspace capacities, traffic demand, and ATFM
580 mitigation strategies. Only then can the full benefit to ATFM operations be
581 achieved.

582 **7. Acknowledgements**

583 We would like to acknowledge the financial support of the Spanish Min-
584 istry of Science, Innovation and Universities under grant RTI2018-098471-B-
585 C32. The project has received funding from the SESAR Joint Undertaking
586 within the framework of the European Union’s Horizon 2020 research and
587 innovation programme under grant agreement No 891965.

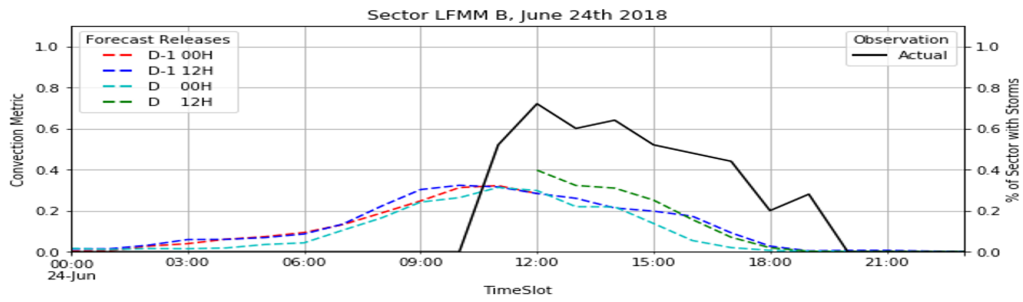
588 **References**

- 589 (2015). *CAE Oxford Aviation Academy METEOROLOGY*. ATPL Ground
590 Training. CAE Oxford Aviation Academy (UK).
- 591 Baldauf, M., Seifert, A., Förstner, J., Majewski, D., Raschendorfer, M.,
592 & Reinhardt, T. (2011). Operational convective-scale numerical weather

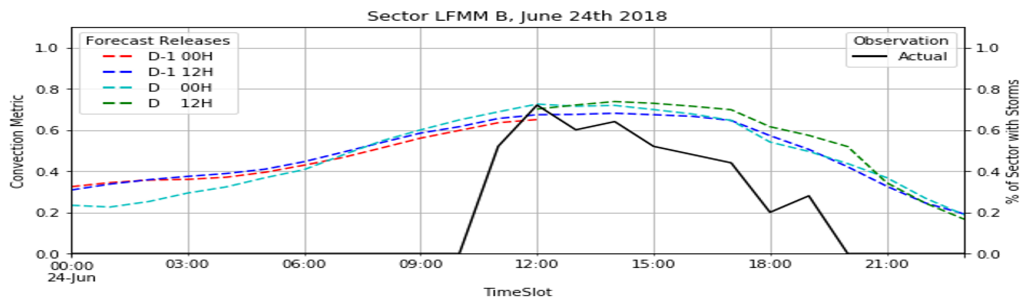
- 593 prediction with the cosmo model: Description and sensitivities. *Monthly*
594 *Weather Review*, 139, 3887–3905.
- 595 Breiman, L. (2001). Random forests. *Machine learning*, 45, 5–32.
- 596 Collins, W., & Tissot, P. (2015). An artificial neural network model to
597 predict thunderstorms within 400 km² south texas domains. *Meteorological*
598 *Applications*, 22, 650–665.
- 599 Cook, A., & Tanner, G. (2015). European airline delay cost reference val-
600 ues.(2015). *Eurocontrol: Brussels, Belgium*, .
- 601 EUROCONTROL (2019). *2018 Performance Review Report, "An Assess-*
602 *ment of Air Traffic Management in Europe during the Calendar Year*
603 *2018"*. EUROCONTROL [https://www.eurocontrol.int/air-navigation-](https://www.eurocontrol.int/air-navigation-services-performance-review)
604 [services-performance-review](https://www.eurocontrol.int/air-navigation-services-performance-review).
- 605 Evans, J. E., & Ducot, E. R. (2006). Corridor integrated weather system.
606 *Lincoln Laboratory Journal*, 16, 59.
- 607 Fisher, A., Rudin, C., & Dominici, F. (2019). All models are wrong, but
608 many are useful: Learning a variable’s importance by studying an entire
609 class of prediction models simultaneously. *Journal of Machine Learning*
610 *Research*, 20, 1–81.
- 611 González-Arribas, D., Soler, M., Sanjurjo-Rivo, M., García-Heras, J., Sacher,
612 D., Gelhardt, U., Lang, J., Hauf, T., & Simarro, J. (2019). Robust optimal
613 trajectory planning under uncertain winds and convective risk. In E. N. R.
614 Institute (Ed.), *Air Traffic Management and Systems III* (pp. 82–103).
615 Singapore: Springer Singapore.
- 616 He, J., & Loboda, T. V. (2020). Modeling cloud-to-ground lightning prob-
617 ability in alaskan tundra through the integration of weather research and
618 forecast (wrf) model and machine learning method. *Environmental Re-*
619 *search Letters*, 15, 115009.
- 620 Khandan, R., Alavipanah, S. K., Biazar, A. P., & Gharaylou, M. (2018).
621 Probabilistic convective initiation nowcasting with reduced satellite-nwp
622 predictors over iran. *Asia-Pacific Journal of Atmospheric Sciences*, 54,
623 431–443.

- 624 Lee, J.-G., Min, K.-H., Park, H., Kim, Y., Chung, C.-Y., & Chang, E.-C.
625 (2020). Improvement of the rapid-development thunderstorm (rdt) algo-
626 rithm for use with the gk2a satellite. *Asia-Pacific Journal of Atmospheric*
627 *Sciences*, *56*, 307–319.
- 628 Li, H., Li, Y., Li, X., Ye, Y., Li, X., & Xie, P. (2019). A comparative study on
629 machine learning approaches to thunderstorm gale identification. In *Pro-*
630 *ceedings of the 2019 11th International Conference on Machine Learning*
631 *and Computing ICMLC '19* (p. 12–16). New York, NY, USA: Association
632 for Computing Machinery.
- 633 Mandrekar, J. N. (2010). Receiver operating characteristic curve in diagnostic
634 test assessment. *Journal of Thoracic Oncology*, *5*, 1315–1316.
- 635 Mecikalski, J. R., Williams, J. K., Jewett, C. P., Ahijevych, D., LeRoy, A.,
636 & Walker, J. R. (2015). Probabilistic 0–1-h Convective Initiation Now-
637 casts that Combine Geostationary Satellite Observations and Numerical
638 Weather Prediction Model Data. *Journal of Applied Meteorology and Cli-*
639 *matology*, *54*, 1039–1059.
- 640 Molteni, F., Buizza, R., Palmer, T. N., & Petroliagis, T. (1996). The ecmwf
641 ensemble prediction system: Methodology and validation. *Quarterly jour-*
642 *nal of the royal meteorological society*, *122*, 73–119.
- 643 Palmer, T., Buizza, R., Hagedorn, R., Lawrence, A., Leutbecher, M.,
644 & Smith, L. (2006). Ensemble prediction: a pedagogical perspective.
645 *ECMWF newsletter*, *106*, 10–17.
- 646 Šaur, D. (2017). Forecasting of convective precipitation through nwp mod-
647 els and algorithm of storms prediction. In R. Silhavy, R. Senkerik,
648 Z. Kominkova Oplatkova, Z. Prokopova, & P. Silhavy (Eds.), *Artificial*
649 *Intelligence Trends in Intelligent Systems* (pp. 125–136). Cham: Springer
650 International Publishing.
- 651 Simon, T., Fabsic, P., Mayr, G. J., Umlauf, N., & Zeileis, A. (2018). Proba-
652 bilistic forecasting of thunderstorms in the eastern alps. *Monthly Weather*
653 *Review*, *146*, 2999–3009.
- 654 Spiridonov, V., Baez, J., Telenta, B., & Jakimovski, B. (2020). Prediction
655 of extreme convective rainfall intensities using a free-running 3-d sub-km-

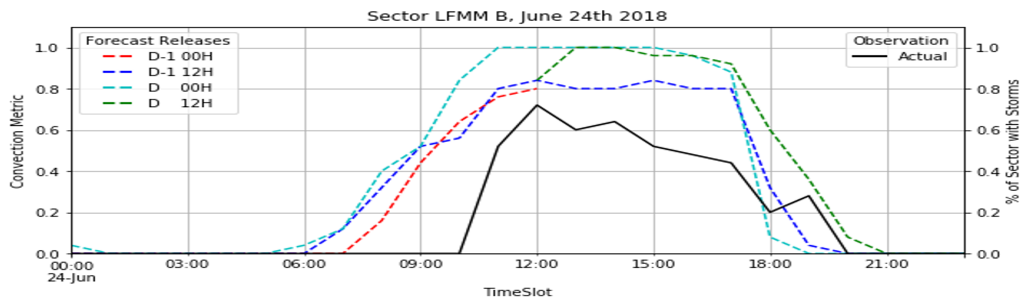
- 656 scale cloud model initialized from wrf km-scale nwp forecasts. *Journal of*
657 *Atmospheric and Solar-Terrestrial Physics*, 209, 105401.
- 658 Srivastava, N., Hinton, G., Krizhevsky, A., Sutskever, I., & Salakhutdinov, R.
659 (2014). Dropout: a simple way to prevent neural networks from overfitting.
660 *The journal of machine learning research*, 15, 1929–1958.
- 661 Wilson, J. W., Crook, N. A., Mueller, C. K., Sun, J., & Dixon, M. (1998).
662 Nowcasting thunderstorms: A status report. *Bulletin of the American*
663 *Meteorological Society*, 79, 2079–2100.
- 664 Zhou, K., Zheng, Y., Li, B., Dong, W., & Zhang, X. (2019). Forecasting
665 different types of convective weather: A deep learning approach. *Journal*
666 *of Meteorological Research*, 33, 797–809.



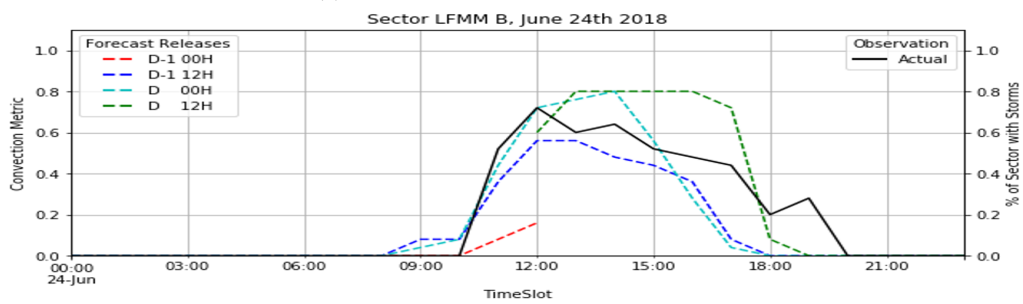
(a) Average value Baseline Indicator



(b) Average value Neural Network Model



(c) Neural Network with threshold of 0.6



(d) Neural Network with threshold of 0.7

Figure 15: Convection metrics evaluating the weather situation in Marseille Sector B for multiple forecast releases.